Journal of Solid State Chemistry **145,** 496–502 (1999)
Article ID jssc.1999.8194, available online at http://www.idealibrary.com on IDEAL®

Structural Properties of the Superconducting Salt $(BEDT\text{-}TTF)_3Cl_2\cdot(H_2O)_2$ at Low Temperatures

Jacques Gaultier,* Sylvie Hébrard-Bracchetti,* Philippe Guionneau,*,[1] Cameron J. Kepert,†,[2] Daniel Chasseau,*,[3] Laurent Ducasse,‡ Yvette Barrans,* Mohamedally Kurmoo,†,[4] and Peter Day†

*Laboratoire des Sciences Moléculaires, Institut de Chimie de la Matière Condensée de Bordeaux, UPR 9048, Université Bordeaux I, 33608 Pessac Cedex, France; †The Royal Institution of Great Britain, 21 Albemarle Street, London, W1X 4BS, United Kingdom; and ‡Laboratoire de Physico-Chimie Moléculaire, UMR 5803, Université Bordeaux I, 33405 Talence Cedex, France
E-mail: chasseau@icmcb.u.bordeaux.fr

Received September 11, 1998; in revised form January 15, 1999; accepted February 2, 1999

The X-ray crystal structure of $(BEDT\text{-}TTF)_3Cl_2\cdot(H_2O)_2$ [BEDT-TTF = bis(ethylenedithio)tetrathiafulvalene] has been determined at 190, 130, and 10 K. The broad metal–insulator transition (100–160 K) observed in the resistivity data at ambient pressure, and the pressure induced superconductivity ($T_c = 5$ K at 1.2 GPa) can be associated with temperature-dependent motion of the molecules within the unit cell and charge redistribution among the three independent BEDT-TTF molecules. The motion can be considered as a dimerization of the BEDT-TTF along the *a*-axis. The thermal expansion tensor in the range 12 to 295 K is anisotropic and reveals no sharp anomaly. The system remains two dimensional at all temperatures, in agreement with the electrical conductivity measurements. © 1999 Academic Press

INTRODUCTION

All the chloride salts of BEDT-TTF ($C_{10}H_8S_8$, bis(ethylenedithio)-tetrathiafulvalene) are found to contain water of crystallization which forms clusters with the chloride ion, thus adopting geometries to fit in the size and shape of the cavities formed by the BEDT-TTF molecules. As a result of this the number of carriers in the conduction band of the organic moiety is variable. For the five structural variants, $(BEDT\text{-}TTF)_4Cl_2\cdot 6H_2O$ (1), $(BEDT\text{-}TTF)_4Cl_2\cdot 4H_2O$ (2), $(BEDT\text{-}TTF)_3Cl_{2.5}\cdot H_5O_2$ (3), $(BEDT\text{-}TTF)_3Cl_2\cdot 2H_2O$ (4), and $(BEDT\text{-}TTF)_3Cl_2\cdot 5H_2O$ (5) the nominal band filling is $\frac{3}{4}$, $\frac{3}{4}$, $\frac{3}{4}$, $\frac{2}{3}$, and $\frac{2}{3}$, respectively. Their crystal structures consist of layers of BEDT-TTF separated by clusters of the hydrated anions. The calculated electronic band structures show bands of narrow widths and predict anisotropic electrical conductivities. Except for the latter, which is a semiconductor, they are all metallic at room temperature and undergo broad second-order transitions from states of high conductivity at high temperature to states of low conductivity at low temperature. Considering the electrical and magnetic data of $(BEDT\text{-}TTF)_3Cl_2\cdot 2H_2O$ it is proposed that the transition is accompanied by a gradual decrease of the density of state at the Fermi level (4). To understand these anomalies, we have performed low-temperature crystallographic studies on two of these salts; the results for $(BEDT\text{-}TTF)_4Cl_2\cdot 6H_2O$ have been already reported (6), and preliminary observations of the low-temperature crystal structure of $(BEDT\text{-}TTF)_3Cl_2\cdot 2H_2O$ based on a rigid body refinement of neutron data has also been reported. Here, we present results of an extensive study of the physical properties of $(BEDT\text{-}TTF)_3Cl_2\cdot 2H_2O$ as a function of temperature, where the crystal structure has been determined with higher precision than in previous studies. These are reported in the following sections.

The structural and physical properties of $(BEDT\text{-}TTF)_3Cl_2\cdot 2H_2O$, one of the most interesting from the point of view of the localization mechanism in charge transfer salts, are of great interest (7, 8); it is the only salt of the chloride series that becomes superconducting under pressure. While the conductivities of most BEDT-TTF salts are lower than $100\,\Omega\,cm^{-1}$, those of the chloride salts are in excess of $500\,\Omega\,cm^{-1}$, and furthermore they present the largest anisotropy. For example the room-temperature conductivities of $(BEDT\text{-}TTF)_3Cl_2\cdot 2H_2O$ along the three crystallographic axes are $\sigma_a = 500$, $\sigma_b = 40$, and $\sigma_c = 0.6\,\Omega\,cm^{-1}$, suggesting quasi-two-dimensional character. The temperature-dependent resistivity of this salt presents a broad minimum centered around 160 K and a sharp

[1] Durham Chemical Crystallography Group, Chemistry Department, South Road, Durham DH1 3LE, United Kingdom.
[2] Inorganic Chemistry Laboratory, South Parks Road, Oxford OX1 3QR, United Kingdom.
[3] To whom correspondence should be addressed.
[4] Institut de Physique et Chimie des Matériaux de Strasbourg, GM1, 23 rue du Loess, 67037 Strasbourg, France.

0022-4596/99 $30.00

increase ca. 100 K. At lower temperatures (50 and 10 K) there is evidence of further plateaus. These anomalies are suppressed on application of pressure and a superconducting state is established at a pressure of 0.8 GPa. The critical temperature increases to ca. 5 K (onset) for a pressure of 1.2 GPa, followed by slow decrease at higher pressures. The phase diagram is typical of organic superconductors such as the family of TMTSF (tetramethyltetraselenafulvalene) salts. Superconductivity is destroyed with a magnetic field greater than 2T. The magnetic susceptibility is weakly temperature dependent above 160 K, and below this temperature it decreases gradually to nearly zero at 60 K.

The title compound has been well known since 1987 when it was synthesized accidentally by three independent groups employing three completely different procedures (4). As a result, there exist three similar crystal structure determinations at room temperature.

The asymmetric unit consists of three independent BEDT-TTF cations, A, B, and C, which are arranged in the structure which can be described by the so-called β'' phase (9). The structure can be viewed in two different ways. Firstly, the three independent BEDT-TTF cations are stacked almost parallel to each other into chains in the ABCABC sequence along b (Fig. 1) and form an angle of 57° with the b axis. The chains alternate along the a direction. Alternatively, this organic network can be described as a succession of sheets along c with alternating layers of $\cdots$ AAAA $\cdots$ and $\cdots$ BCBC $\cdots$. The intrastack interactions are weak compared to some of the interstack ones, in agreement with the physical behavior. Four chlorides anions and four water molecules form a cluster (Fig. 2) which lies between the BEDT-TTF sheets in the ab plane. The anionic network is stabilized by strong hydrogen bonds *viz.* O–H $\cdots$ Cl and O–H $\cdots$ O.

The metal–insulator (MI) transition could be due to the formation of a charge density wave (CDW) and therefore characterized by well-defined superlattice reflections or lines having a known wave vector. Alternatively, it may be due to temperature-dependent gradual charge transfer between the different independent donor molecules causing electronic localization. Low-temperature fixed crystal X-ray diffuse scattering experiments fail to identify any superlattice reflection due to a long-range order. A previous elastic neutron scattering experiment at 50 K on a single deuterated crystal also did not reveal any long-range order (10). The structure was refined from these data to a high reliability factor ($R = 0.16$) starting from the room temperature atomic coordinates and employing a rigid BEDT-TTF. To go further in the understanding of the behavior of this salt, we performed the low temperature X-ray diffraction study from room temperature to 10 K. This investigation has been carried out at Bordeaux with a classical X-ray source, and a complementary experiment has been done at the European Synchrotron Radiation Facility (ESRF).

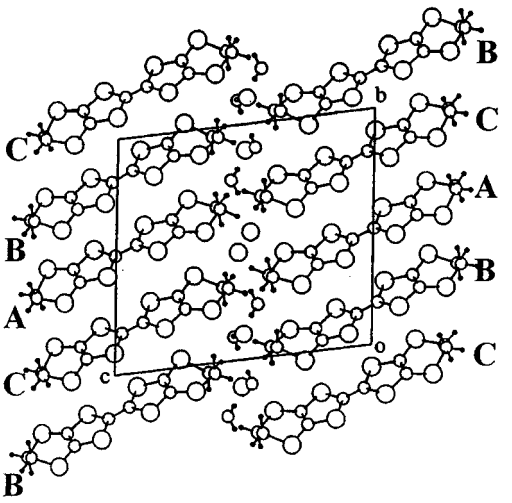

FIG. 1. View of the crystal structure of $ET_3Cl_2 \cdot 2(H_2O)$ along a.

EXPERIMENTAL

The low-temperature investigation has been performed on a 3-circle diffractometer equipped with a closed cycle cryostat, as described previously (11). This apparatus allows us to reach 10 K with a precision of 1 K. The sample is mounted on a copper tip which is placed on the cold finger of the cryostat. The sample is then sealed in a beryllium can containing helium exchange gas. The whole assembly is then surrounded by a Mylar thermal shield and the beryllium vacuum shroud.

Two different single crystals have been used for the crystal structure study. The first one was used for the 130 and 10 K investigations. The second crystal was used to study the temperature dependence of the cell parameters on warming it from 12 to 295 K for 26 different temperatures and to collect the diffraction intensities at 190 K for the crystal structure determination. In the latter case, accidental fluctuation of the temperature prevented us from obtaining a homogeneous set of intensity reflections. Consequently, the results are less accurate. The cell parameters were derived from 13 accurately measured strong Bragg reflections.

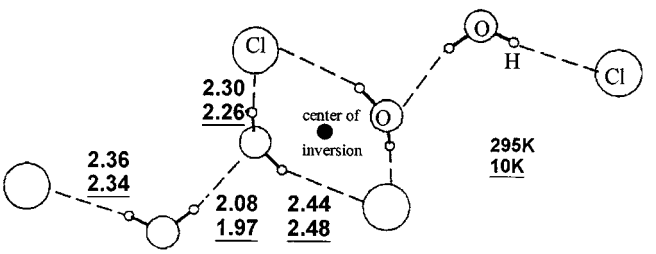

FIG. 2. Anionic motif and the shortest interatomic distances (Å) at room temperature and 10 K.

TABLE 1
Crystal and Experimental Data

Temperature	190 K[a]	130 K[a]	10 K[a]	295 K[b]
Dimension (mm)	0.7×0.5×0.04	0.4×1.1×0.04	0.4×1.1×0.04	0.4×0.15×0.03
Diffractometer		3 circle (Mo$K\alpha$)		4 circle (Cu$K\alpha$)
Space group	$P\bar{1}$	$P\bar{1}$	$P\bar{1}$	$P\bar{1}$
Z (ET/Cell)	2 (6)	2 (6)	2 (6)	2 (6)
a (Å)	11.183 (2)	11.164 (2)	11.125 (2)	11.214 (2)
b (Å)	13.746 (2)	13.686 (2)	13.655 (2)	13.894 (2)
c (Å)	15.904 (2)	15.933 (2)	15.938 (2)	15.904 (2)
α (°)	94.95 (1)	95.00 (1)	95.13 (1)	94.74 (1)
β (°)	109.50 (1)	109.72 (1)	109.86 (1)	107.27 (1)
γ (°)	96.89 (1)	96.66 (1)	96.57 (1)	97.03 (1)
Volume (Å^3)	2267 (1)	2256 (1)	2240 (1)	2304 (1)
D_{calc} (g cm^{-3})	1.847	1.856	1.869	1.807
$F(000)$	1288	1288	1288	1288
Refl. measured	7337	7092	7713	12614
Refl. independ.	6551	6633	7228	9467
Refl. used	4519	5220	6031	6013
$I/\sigma(I)$	2	2.5	2.5	3
Correct. absorp.	No	No	No	Yes
R_{int} (%)	3.6	2.9	2.0	?
R	0.060	0.048	0.040	0.045
wR	0.047	0.039	0.035	0.041

[a] This work.
[b] Reference (4c).

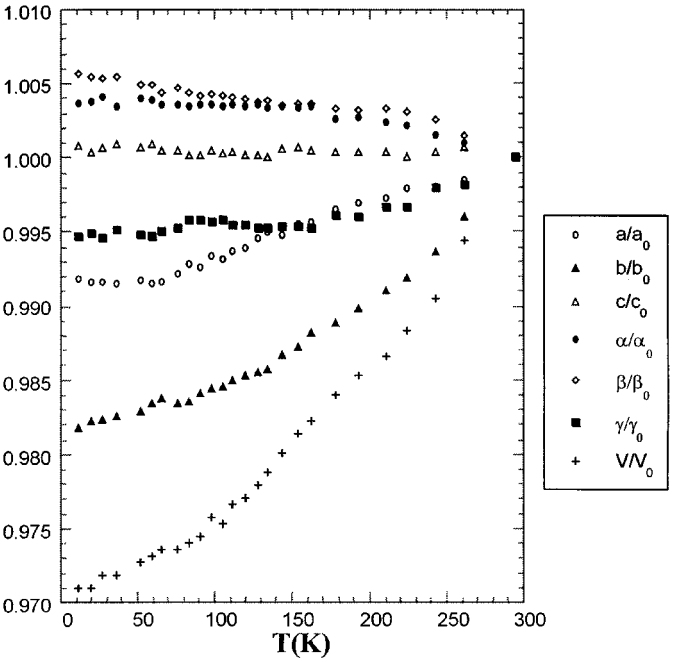

FIG. 3. Relative evolution of the cell parameters as a function of the temperature of $ET_3Cl_2 \cdot (H_2O)_2$.

Crystal structure refinements were performed departing from the room-temperature atomic coordinates (Table 1) and using the local program AFCRIS with a "Robust-Resistant" weighting scheme. This allows us to minimize the contribution of the reflections whose intensity might be altered by the scattering of the beryllium containers. No absorption correction was applied. All the thermal atomic parameters of the nonhydrogen atoms were anisotropically refined. The coordinates of the hydrogen atoms of both BEDT-TTF cations and water molecules were found from the Fourier-difference syntheses.

The experiment at the ESRF (beamline 2, ID11) was performed in order to check eventual modifications of the lattice, unobservable using classical techniques. The apparatus provided was a Displex continuous-flow helium cryostat fitted with five Mylar windows separated by aluminum struts. Image plate detectors were employed. A series of ϕ scans of 10° oscillation was performed at 15 K.

RESULTS AND DISCUSSION

Temperature Dependence of the Cell Parameters

The temperature-dependence of the cell parameters (Fig. 3) is strongly anisotropic, as often observed for the BEDT-TTF salts; the relative variations $\Delta(l)/[l\Delta(l)]$, $l = a, b, c$, of the three parameters show this anisotropic thermal expansion from 12 to 295 K $[2.9, 6.4, 0.3] \times 10^{-5}\,K^{-1}$. The b parameter, which corresponds to the BEDT-TTF stacking axis, increases approximately three times more than the a parameter, corresponding to the interstack direction. Such a difference in thermal expansion of intrastack and interstack is quite common and already observed in (BEDT-TTF)$_4Cl_2 \cdot 6H_2O$, (6) α'-(BEDT-TTF)$_2Ag(CN)_2$ (12), α'-(BEDT-TTF)$_2AuBr_2$ (11), and (BEDT-TTF)$_3CuBr_4$ (13). The c parameter, corresponding almost to the BEDT-TTF molecular axis and the perpendicular to the layers, does not change with temperature. The 3% increase of the cell volume from 12 to 295 K is similar to the corresponding data in the four salts mentioned above. For these α'-(BEDT-TTF)$_2X$ and (BEDT-TTF)$_3CuBr_4$ salts, the volume contraction on cooling from 300 to 12 K is equivalent to the contraction obtained when applying a pressure of around 0.5 GPa.

Temperature evolution of the cell parameters reveals no sharp anomaly, although a very slight change in the curves occurs within the temperature range 150–180 K. The latter is, however, within the standard deviations and was therefore ignored for the calculation of the thermal expansion tensor. The coordinates of the vectors α_1, α_2, and α_3 of such a tensor are reported in Table 2. For all temperatures, the direction of the principal thermal expansion, α_1, is close to the crystallographic b axis; the angle between these two directions decreases slightly from 24.2° at 12 K to 15.9° at 295 K while the direction of thermal expansion rotates by 32° around b. The α_2 and α_3 directions almost lie within the

TABLE 2
Coordinates of the Three Principal Thermal Expansion Tensorial Vectors (in Å)

	α_1	α_2	α_3
12 K	$\begin{pmatrix} +0.112 \\ -0.893 \\ +0.369 \end{pmatrix}$	$\begin{pmatrix} +1.067 \\ +0.283 \\ +0.411 \end{pmatrix}$	$\begin{pmatrix} +0.080 \\ -0.394 \\ -0.919 \end{pmatrix}$
130 K	$\begin{pmatrix} +0.231 \\ -0.944 \\ -0.077 \end{pmatrix}$	$\begin{pmatrix} +1.021 \\ +0.343 \\ +0.620 \end{pmatrix}$	$\begin{pmatrix} +0.245 \\ +0.158 \\ -0.870 \end{pmatrix}$
295 K	$\begin{pmatrix} +0.181 \\ -0.952 \\ -0.158 \end{pmatrix}$	$\begin{pmatrix} +0.998 \\ +0.256 \\ +0.724 \end{pmatrix}$	$\begin{pmatrix} +0.378 \\ +0.249 \\ -0.770 \end{pmatrix}$

ac crystallographic plane. The angles between these two directions and the BEDT-TTF molecular planes decrease from 12.1°to 2.5° and from 50.6° to 21.9° for α_2 and α_3, respectively. Therefore the principal directions of thermal expansion α_1, α_2, and α_3 correspond to the intrastack interactions, to the transverse interactions and to the interactions between the BEDT-TTF layers and the anionic layers, respectively. The amplitudes corresponding to these directions increase almost linearly with temperature (Fig. 4). The amplitude of α_1 is less than that of α_2 at 12 K, but increases by a factor of 6 to become larger than α_2 at 80 K, suggesting that the large intrastack spaces are more affected by the temperature change than the interstack ones. The negative values of the α_3 amplitude correspond to a Poisson contraction: it denotes a contraction as the temperature increases in this direction even if here, the phenomenon appears too weak to be significant.

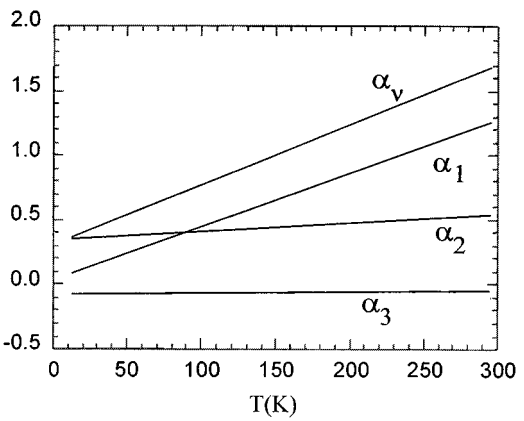

FIG. 4. Amplitudes of principal dilatation ($10^{-4}\,K^{-1}$) in $ET_3Cl_2 \cdot (H_2O)_2$.

The bulk modulus (α_v^{-1}) reflects the thermal expansion character of the salt: the smaller the value the more deformable is the cell. For this salt, the value at 100 K (12,700 K) is similar to that of $(BEDT\text{-}TTF)_3CuBr_4$ (11,200 K) and higher than those of the α′-$(BEDT\text{-}TTF)_2X$ salts (∼8100 K) while at room temperature (5800 K) it is lower (9000 and 6000 K, respectively). The title compound appears quite deformable at room temperature, the main part of the contraction already done at 100 K when the crystal becomes poorly deformable. In fact, as far as the cell evolution is concerned, the transition to a less conducting state at 100 K appears continuous in this case, contrary to the changes observed in the cell of the α′-$(BEDT\text{-}TTF)_2X$ and $(BEDT\text{-}TTF)_4Cl_2 \cdot 6H_2O$ salts (doubling of one parameter and change of space group for the latter).

A preliminary experiment at the ESRF revealed the presence at 15 K of over 50 reflections at $a^*/2$. The reflections intensities were very weak (< 1% of the Bragg reflections), unobservable using classical X-ray equipment. Further analyses of these data were not possible due to contamination of the intensity and deformation of the spots with intense diffraction rings from the aluminum struts. Further experiments are envisaged to determine the temperature dependence of these reflections. In any case, a doubling of the cell along *a* should not change the space group but may mean the presence of six independent BEDT-TTF molecules per cell.

Intramolecular BEDT-TTF Conformation

The three independent molecules are very similar to one another at room temperature and their geometries change slightly as a function of temperature. The first observation is the freezing out of the strong disorder of he two ethylene groups of the BEDT-TTF. This disorder is shown by the shortening of the C–C bond lengths compared to the expected value (1.52 Å) and an increase of the S–C–C angles by 4–5° from the normal value (114°). At 300 K, the two ethylene extremities of A are disordered (1.446(8) Å; 1.384(8) Å), one of B (1.505(8) Å; 1.410(8) Å) while those of C are almost ordered (1.496(8) Å; 1.475(8) Å). This disorder disappears continuously as the temperature decreases: at 190 K the extremities of B are ordered (1.53(1) Å; 1.51(2) Å), but those of A remain disordered (1.46(1) Å; 1.40(2) Å); the latter is ordered at 10 K (1.519(6) Å; 1.484(9) Å). The same conclusion can be reached from examination of the thermal parameters, B_{eq}, since the high values for B and A extremities at high temperature ($B_{eq} > 5$ Å^2) decrease to normal ones at 10 K ($B_{eq} < 1$ Å^2). The value of $B_{eq} \sim 1.5$ Å^2 for one of the extremities of A suggests it is still thermally activated. Therefore, the disorder of the ethylene extremities can be considered as dynamic. Such an observation appears to be common for many of the $(BEDT\text{-}TTF)_mX_n$ compounds.

TABLE 3
Intramolecular Averaged Bond Lengths (Å) and Estimated Charges (Q_{calc})

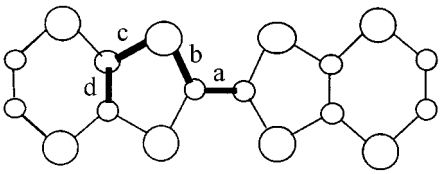

ET	T (K)	a	b	c	d	Q_{calc}
A	295	1.385	1.726	1.745	1.354	0.85
	130	1.381	1.728	1.746	1.369	0.91
	10	1.385	1.728	1.749	1.371	0.96
B	295	1.376	1.732	1.746	1.354	0.73
	130	1.376	1.734	1.749	1.359	0.85
	10	1.386	1.731	1.749	1.361	0.88
C	295	1.375	1.734	1.747	1.347	0.66
	130	1.377	1.739	1.751	1.349	0.61
	10	1.370	1.744	1.756	1.353	0.54

The intramolecular bond lengths, a, b, c, and d (Table 3), of the central TTF backbone of the three crystallographically independent BEDT-TTF cations are similar at room temperature. On cooling, those of A and B approach each other and become nonequivalent to those of C. Using an empirical statistical method developed (14) and utilized successfully (6, 12, 15) to predict the charge carried by the cations, we have estimated to an accuracy of $\pm 10\%$ the charge (Q_{calc}) on the BEDT-TTF cations at the different temperatures (Table 3).

The charge of the molecules depends on temperature: the charges on A and B are close to one another (the first one being slightly higher) and increase on lowering the temperature while the charge on C is lower than the other two and decreases at low temperature. This result infers that on lowering the temperature a gradual charge localization takes place. This effect has previously been observed for other BEDT-TTF salts. We may conclude that this charge localization drives the broad transition from a highly conducting state to a less conducting state. We remark that the sums of the positive charges (2.24, 2.37, and 2.38 at 295, 130, and 10 K, respectively) on the three BEDT-TTF cations are slightly higher than the expected value of $2+$, but are within the estimated error of calculation.

Low Temperature Crystal Structure

The features of the crystal structure are conserved at all the temperatures studied.

Anionic Motif

The anionic repeat unit consists of two chlorine anions and two water molecules and their homologous through a center of inversion, the stability being assumed by strong hydrogen bonds (Fig. 2). This motif is fairly planar. There are no significant changes in the interatomic distances and angles on cooling from 295 to 10 K.

The interactions between the anionic and cationic network are created through the ethylene extremities, the chloride anions and the water molecules. The three BEDT-TTF entities do not possess the same anionic environment. One of the chloride ions is closer to A, and the other is closer to B and C. The distances between the BEDT-TTF extremities and the anionic motif decrease continuously in an homogeneous manner with the temperature, the C $\cdots$ Cl and C $\cdots$ O decreasing by ~ 0.1 Å and the CH $\cdots$ O by ~ 0.06 Å. These interactions might have an influence on the charge distribution. It is more and more likely in this class of compounds that electrostatic pairwise interactions between the cations and the anions may be responsible for one of the mechanisms for localization. The stability, charge distribution and compactness of the anionic motif may be responsible for driving the packing of the BEDT-TTF molecules, through optimization of the hydrogen bond network between the anionic unit and the BEDT-TTF molecules.

Crystal Packing

The interaction between two BEDT-TTF molecules could be characterized by four parameters: the averaged distances between them (d), the translational shifts of the center of gravity of the molecular centers (normal ΔX, and parallel, ΔY) and the angle (θ) between the two molecular

TABLE 4
Geometrical Parameters[a] Defining the Intrastack Interactions

		295 K	130 K	10 K
	ΔX	+ 1.853	+ 1.879	+ 1.902
	ΔY	− 3.195	− 3.126	− 3.106
S1	d	3.93	3.82	3.80
	θ	3.3	3.3	3.3
	ΔX	+ 1.973	+ 1.936	+ 1.917
	ΔY	− 2.920	− 2.914	− 2.912
S2	d	3.84	3.76	3.73
	θ	3.7	3.1	3.4
	ΔX	− 1.788	− 1.788	− 1.811
	ΔY	+ 0.270	+ 0.290	+ 0.296
S3	d	3.93	3.85	3.82
	θ	0.2	0.2	0.4

[a] ΔX, ΔY, and d are in Å, and θ is in degrees.

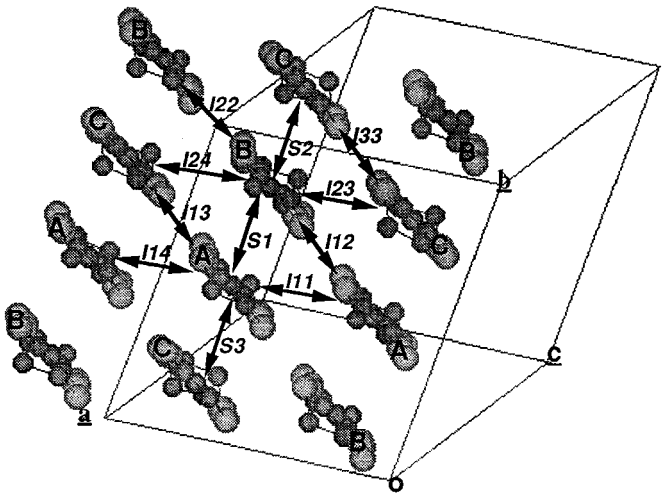

FIG. 5. View of a conducting sheet and nomenclature of the intermolecular interactions in $ET_3Cl_2 \cdot (H_2O)_2$.

TABLE 5
Temperature Dependence of the Calculated Transfer Integrals (t/meV)

t (meV)	295 K	190 K	130 K	10 K
t_{I11}	168	166	162	156
t_{I23}	175	170	163	160
t_{I14}	194	198	204	210
t_{I24}	196	202	205	206
t_{S1}	− 21	− 28	− 32	− 37
t_{S3}	− 24	− 27	− 31	− 36
t_{S2}	− 59	− 69	− 80	− 85
t_{I33}	− 66	− 67	− 69	− 71
t_{I13}	− 91	− 95	− 98	− 100
t_{I12}	− 99	− 109	− 112	− 114
t_{I22}	− 76	− 85	− 89	− 94

axes. The packing of the BEDT-TTF in this salt defines three overlaps S1 (AB), S2 (BC), and S3 (AC). Their relative orientations are not favourable for strong interactions (Table 4) due to the long d distances. This is reflected in the conductivity measurements where it is intermediate along the stacking axis b. These distances increase continuously with the temperature while the other parameters (ΔX, ΔY, and θ) are only slightly temperature dependent.

The interstack interactions are defined by eight interactions: I11, I14, I23, and I24 along the [110] direction and I12, I13, I22, and I33 along the [320] direction (Fig. 5). The first four are similar to each other at room temperature and the short S ⋯ S contacts, less than the sum of the van der Waals radii, predict strong interactions. The distances increase for I11 and I23 (+0.07 Å) while they decrease for I14 and I24 (−0.06 Å) from 295 to 10 K. The four other interactions develop few short contacts between the BEDT-TTF and the angles of contact correspond to antibonding interactions. These interactions increase slightly at low temperature (distances shortened by ∼0.05 Å). Thus, we can predict an increase of most of the interactions, a slight dimerization being introduced by the difference in behavior of I11, I23 and I14, I24. In order to quantify these changes we have calculated the electronic interactions.

Electronic Interactions

The transfer integrals (Table 5) have been calculated using the extended-Hückel method employing double-ζ basis sets (16). The values confirm the predictions made from the structural analysis; the intrastack interactions are weak and increase slightly at low temperature. The antibonding interactions I12, I22, I13, I33 are of the same order of magnitude and increase continuously with lowering temperature. The strong transverse interactions I11 and I23 decrease while I14 and I24 increase.

The tight-binding electronic band structures have been calculated at 295 and 10 K (Fig. 6). The six bands span an energy of 1.3 eV and the fourth and fifth bands cross the Fermi level and describe a Fermi surface consisting of both one dimensional sections and two dimensional pockets, the cross over energy between the 1D and 2D sections being very small. The size of the pocket is reduced and the density of states at the Fermi energy is lowered at low temperatures. The conduction properties of this salt are not consistent

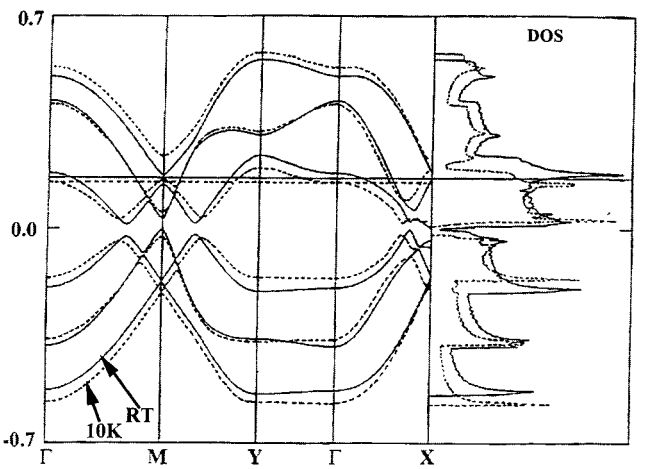

FIG. 6. Band structure at room temperature and 10 K (dot lines) of $ET_3Cl_2 \cdot (H_2O)_2$.

with the metallic character deduced from the one-electron picture used in the band structure calculation. Actually, the localization observed in this salt is reminiscent of the situation met in many other 1D and 2D systems. The influence of electron–electron correlation may be certainly important to explain these behaviors. A valence-bond picture of the electronic properties (17) has shown that the dimerization of the interactions along the stack in quasi 1D compounds may be considered as the pertinent parameter related to the metal–insulator transition. This model may be also applied to 2D BEDT-TTF salts, like $(BEDT\text{-}TTF)_2AuBr_2$ (11), where a very strong dimerization (3.0) is related to a high-temperature insulating state. In $(BEDT\text{-}TTF)_3Cl_2 \cdot 2H_2O$ we may define a degree of dimerization found in the TMTTF salts with octahedral anions (1.5) for which the temperature of the minimum of resistivity is around 100 K.

CONCLUSION

The metal–insulator transition observed for $(BEDT\text{-}TTF)_3Cl_2 \cdot 2H_2O$ between 100 and 160 K is not accompanied by a dramatic modification of the crystal structure. The cooling down of the crystal results in decrease of the intermolecular distances, ordering of the ethylene extremities of the BEDT-TTF and most importantly, in a variation of the bond lengths due to redistribution of charges. The transition from a metallic state toward a less conducting one is continuous. This work confirms the previous conclusion (18) that decreasing the temperature lowers the density of states at the Fermi level. The localization of the charges observed when lowering the temperature is consistent with the low T insulating ground state. This localization may be prevented by application of pressure thus explaining that the conducting state remains over the whole temperature range before the superconducting ground state occurs.

Further work is needed to confirm the superlattice structure observed by the synchrotron experiment.

Crystallographic data under pressure are needed, as this salt behaves as a superconductor at high pressure ($T_c = 5$ K, $P = 1.2$ GPa). We have recently determined the crystal structure under pressure *and* low temperature of two molecular satls using the same low-temperature device as for the present study associated with a high-pressure cell (19). That may allow some new very interesting investigations, especially on this series of materials.

ACKNOWLEDGMENTS

This work was supported by the European Union (HCM Network) and the Conseil Régional d'Aquitaine. We are grateful to the ESRF for providing us beam time (beamline 2, ID11).

REFERENCES

1. (a) M. B. Inoue, M. A. Bruck, M. Carducci, and Q. Fernando, *Synth. Met.* **38,** 353 (1990). (b) M. J. Rosseinsky, M. Kurmoo, P. Day, I. R. Marsden, R. H. Friend, D. Chasseau, J. Gaultier, G. Bravic, and L. Ducasse, *J. Mater. Chem.* **3**(8), 801 (1993).
2. R. P. Shibaeva, R. M. Lyubovskaya, L. P. Rozenberg, L. I. Buravov, A. A. Ignatiev, N. D. Kushch, E. E. Laukhina, M. K. Makova, E. B. Yabubskii, and A. V. Zvarykina, *Synth. Met.* **27,** A189 (1988).
3. H. Mori, I. Hirabayashi, S. Tanaka, and Y. Maruyama, *Bull. Chem. Soc. Jpn.* **66,** 2156 (1993).
4. (a) T. Mori and H. Inokuchi, *Chem. Lett.* 1657 (1987). (b) M. J. Rosseinsky, M. Kurmoo, D. R. Talham, P. Day, and D. Chasseau, *J. Chem. Soc. Chem. Commun.* 88 (1988). (c) S. D. Obertelli, I. R. Marsden, R. H. Friend, M. Kurmoo, M. J. Rosseinsky, P. Day, F. L. Pratt, and W. Hayes, *in* "Physics and Chemistry of Organic Superconductors" (G. Saito and S. Kagoshima, Eds.), Springer Proceedings in Physics, Vol. 51, p. 272. Springer, Berlin, 1990.
5. G. Ono, A. Izuoka, T. Sugawana, and Y. Sugawana, *Mol. Cryst. Liq. Cryst.* **285,** 63 (1996).
6. P. Guionneau, C. J. Kepert, M. J. Rosseinsky, D. Chasseau, J. Gaultier, M. Kurmoo, M. B. Hursthouse, and P. Day, *J. Mater. Chem.* **8,** 367 (1998).
7. M. Kurmoo, M. J. Rosseinsky, P. Day, P. Auban, W. Kang, D. Jerome, and P. Batail, *Synth. Met.* **27,** A425 (1989).
8. W. Lubczynski, J. Caufield, J. Singleton, W. Hayes, M. Kurmoo, and P. Day, *Synth. Met.* **70,** 835 (1994).
9. J. M. Williams, J. R. Ferraro, R. J. Thorn, K.D. Carlson, U. Geiser, H.H. Wang, A. Kini, and M. H. Whangbo, "Organic Superconductors (Including Fullerene)." Prentice Hall, Englewood Cliffs, NJ, 1992.
10. G. Bravic, D. Chasseau, J. Gaultier, M. J. Rosseinsky, M. Kurmoo, P. Day, and A. Filhol, *Synth. Met.* **42,** 2035 (1991).
11. D. Chasseau, J. Gaultier, G. Bravic, L. Ducasse, M. Kurmoo, and P. Day, *Proc. R. Soc. London A* **442,** 207 (1993).
12. P. Guionneau, M. Rahal, G. Bravic, J. Gaultier, J. M. Mellado, D. Chasseau, L. Ducasse, M. Kurmoo, and P. Day, *J. Mater. Chem.* **5,** 1639 (1995).
13. P. Guionneau, J. Gaultier, D. Chasseau, G. Bravic, Y. Barrans, L. Ducasse, D. Kanazawa, P. Day, and M. Kurmoo, *J. Phys. I France* **9,** 1581 (1996).
14. P. Guionneau, C. J. Kepert, D. Chasseau, M. R. Truter, and P. Day, *Synth. Met.* **86,** 1973 (1997).
15. E. Coronado, J.R. Galán-Mascarós, C. Giménez-Saiz, C. J. Cómez-Garcia, C. Rovira, J. Tarrés, S. Triki, and J. Veciana, *J. Mater. Chem.* **8**(2), 313 (1998).
16. L. Ducasse and A. Fritsch, *Solid State Commun.* **91,** 201 (1994).
17. A. Fritsch and L. Ducasse, *J. Phys. I France* **1,** 855 (1991).
18. M. J. Rosseinsky, Ph.D. Thesis, Oxford University, Oxford, 1990.
19. D. Le Pevelen, Y. Barrans, J. Gaultier, and D. Chasseau, *in* "Proceedings of the International Conference on Synthetic Metals 1998," *Synth. Met.*, in press (1999).